ELSEVIER

Nuclear Instruments and Methods in Physics Research A 410 (1998) 220–228

NUCLEAR INSTRUMENTS & METHODS IN PHYSICS RESEARCH Section A

A full-integrated pulse-shape discriminator for liquid scintillator counters[1]

O. Barnabà, Y.B. Chen, G. Musitelli, R. Nardò, G.L. Raselli*, M. Rossella, P. Torre

Istituto Nazionale di Fisica Nucleare (INFN) sezione di Pavia and Dipartimento di Fisica Nucleare e Teorica, Università di Pavia, via Bassi 6, I-27100 Pavia, Italy

Received 29 January 1997; received in revised form 24 November 1997

Abstract

A low-cost high-performance pulse-shape discriminator for neutron–gamma discrimination using liquid scintillation counters equipped with two photomultipliers is developed. Two independent methods of pulse-shape discrimination are exploited to achieve an optimum neutron–gamma identification. The circuit is especially designed to study the low-intensity neutron background field in the Gran Sasso underground laboratory. A detailed layout and the main performances of the electronic circuit are described.

1. Introduction

A new measurement of the neutron background field in the Gran Sasso laboratory is needed in order to discriminate the background signals from those produced by rare events such as neutrino interactions in large volume devices, like the ICARUS 600 ton detector [1].

In underground laboratories, neutrons may be produced by cosmic-ray interactions in the last few meters of the rock and by spontaneous fission and/or α, n reactions induced by radioactive materials contained in the rock itself. This second source generates the majority of fast neutrons, since, in practice, all the high-energy particles producing neutrons in the atmosphere are absorbed by the rock.

Monte Carlo simulation of the Hall C environment suggests a neutron energy distribution similar to that of a fission spectrum [2]. Moreover, preliminary measurements in the Gran Sasso laboratory give a very low upper limit in the neutron flux ($\approx 10^{-6}\,cm^{-2}\,s^{-1}$), at least five orders of magnitude lower than the value of the natural gamma ray field [3–7].

The ideal spectrometer to study the background neutron energy distribution should have a big sensitive mass, a high neutron detection efficiency and good energy resolution in a wide energy range, low sensitivity to gamma radiation and simple electronics. Although now there is nothing in approaching it, improvements have been made in the performance of organic scintillator proton-recoil

* Corresponding author. E-mail: gianluca.raselli@pv.infn.it.

[1] The work reported here has been done within the ICARUS collaboration.

0168-9002/98/$19.00
PII S0168-9002(98)00200-9

spectrometers. To achieve the required neutron–gamma discrimination sensitivity the Pulse-Shape Discrimination (PSD) technique, with both Zero-Cross Timing (ZCT) and Digital Charge Comparison (DCC) methods [8], has been already used in the Gran Sasso laboratory [5–7]. Such measurements, carried out for few days using few litres of liquid scintillator, report only upper limits on the neutron flux.

For a better knowledge of the neutron energy spectrum new measurements are needed. To reach an acceptable statistical accuracy some tens of litres of liquid scintillator and several months of data taking are required. Nevertheless, a single large volume scintillator counter is not useful for this purpose, because multiscattering of neutrons and light attenuation and dispersion due to a long transmission path in the cell have a negative influence on the PSD performance [9]. On the other hand, neutron detectors equipped with an array of small scintillators cells require complicated and expensive electronics.

A low-cost electronic board is designed and realised for a neutron multidetector consisting of 32 cells, each filled with 11 of liquid scintillator, recently proposed to perform neutron flux and energy spectrum measurements in the Gran Sasso Hall C [2]. The different electronic stages used to accomplish ZCT and DCC pulse-shape discriminations are integrated in a standard single-width NIM module. Results are presented for discriminating between neutron and gamma rays with a $\frac{1}{3}$1 cell filled with liquid scintillator BC501A^{TM}, which shows excellent pulse-shape discrimination properties and is almost universally adopted as standard scintillator for neutron spectrometry [10].

2. Principle of operation

The neutron energy spectrum, as concerns liquid scintillator proton-recoil spectrometers, is computed by unfolding the light pulse height distribution of the incident neutron interactions [11].

In a cylindrical counter the scintillation light is attenuated by reflections on the cell walls and by absorption in the walls or in the scintillator itself. This gives rise, in principle, to a position-dependent light collection and time response, leading to a poor energy resolution and to a neutron–gamma discrimination inefficiency. These problems can be sufficiently reduced by optimising the cell geometry and by collecting the scintillation light at both ends of the counter [12]. Moreover, a compensation of the position-dependent time response can be easily obtained by the use of constant fraction discriminators and meantimer units.

In this regard, a basic electronic set-up is presented in Fig. 1. Scintillation light is detected by two photomultipliers (PMT1 and PMT2) the anode current signals of which are summed by a linear Fan-in/Fan-out. This unit provides three current outputs, one of which is connected to the input of a ZCT PSD. An identification logic flag is provided by this stage every time a neutron interaction occurs in the detector. The remaining current outputs are fed to the inputs of two analog-to-digital converters (ADC) used as charge integrators. The comparison between the total charge obtained by integration of the whole pulse shape, and the delayed charge obtained by integration of the pulse tail, allows DCC pulse-shape discrimination and neutron energy spectrum calculation. Two constant-fraction discriminators (CFD) are used to set the minimum energy deposition of interacting particles. A meantimer unit (MT), used to generate the PSD strobe, performs the time-compensated coincidence of the two CFD signals.

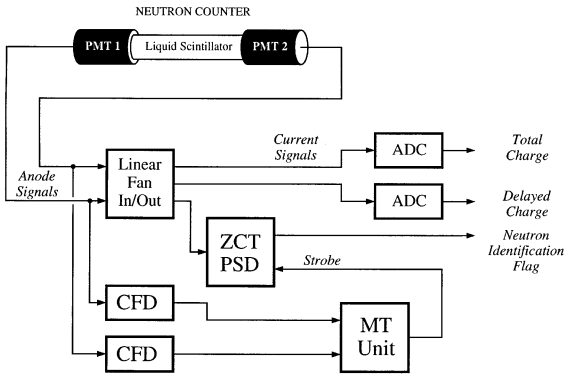

Fig. 1. Block diagram of a basic PSD electronics set-up.

3. PSD Unit, circuit details

Fig. 2 shows the PSD Unit prototype. To lower the costs in multidetector arrays and reduce cables connection in the system, the Fan-in/Fan-out, CFD and PSD stages are all compactly mounted in a standard single-width NIM module. The unit, realised with basic ECL electronic circuits, consists of three main parts: analog front-end, CFD and PSD.

3.1. Analog front-end

The analog front-end, as shown in the block diagram of Fig. 3, sends through the anode signals directly to the other section of the module and sums them into a single current signal.

First of all input anode signals are attenuated using removable 50 Ω resistive attenuators and then summed together by a passive mixer before entering the succeeding amplifier (A1). The attenuation value can be chosen in relation to the gain of the photomultipliers and to the required energy range of the detecting particles. An adjustable DC level (±20 mV) is added to the input of A1 in order to compensate the baseline of the current outputs.

The amplifier A1, a current feedback amplifier AD8001, can drive three 50 Ω output lines, one internally connected to the PSD stage, and the other two externally available for charge measurements. The voltage gain of the amplifier assures the reproduction, in each line, of the linear sum of the two PMTs' signals without appreciable distortion and noise. The good linearity within 1.2 V range represents a good performance for the use with conventional integrating analog-to-digital converters.

Two voltage follower amplifiers AD8002 (A2 and A3) which present high input impedance (10 MΩ) and are able to drive 50 Ω output lines, allow to obtain ideal impedance match and to reduce distortions and reflections.

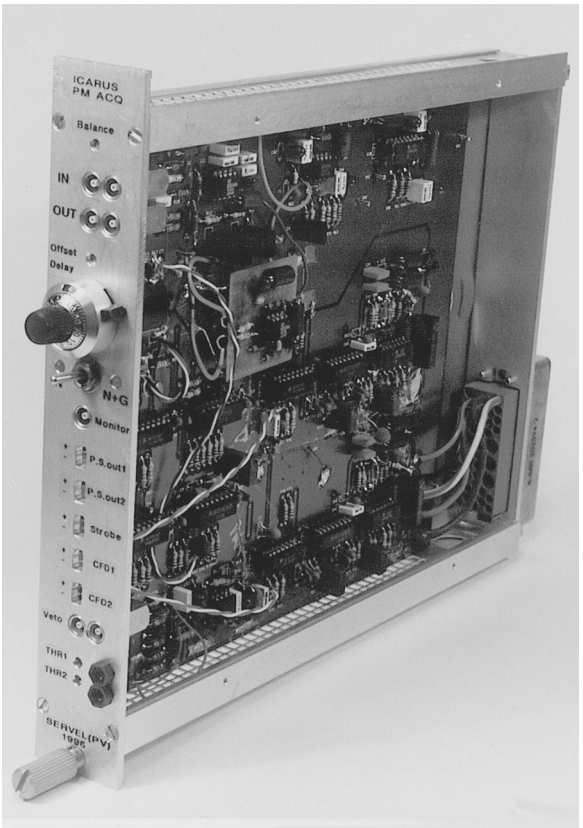

Fig. 2. PSD unit prototype.

3.2. Constant fraction discriminator

For each photomultiplier, a time-walk-compensated ECL logic pulse is provided when the amplitude of the input signals crosses a desired threshold. This operation is accomplished by a Leading Edge Triggering Discriminator (LETD), a CFD and a Pulse Former (FF1). The block diagram relative to one of the two channels of the module is shown in Fig. 4.

The LETD (A5), an ultrafast comparator AD96687, selects pulses the amplitude of which crosses a desired discrimination level. The threshold ranges from − 20 mV to − 1 V and can be adjusted locally by a front-panel potentiometer. A monitor point permits the measurement with a voltmeter. The anticoincidence between the LETD output and the veto line, which can be externally driven by a NIM logic level, is formed by the logic gate G1. A correct use of the veto facility as regards pile-up rejection can strongly improve the performance of the PSD circuit at high event rates [13].

The CFD is realised with a second ultrafast comparator AD96687 (A4) used as a differential

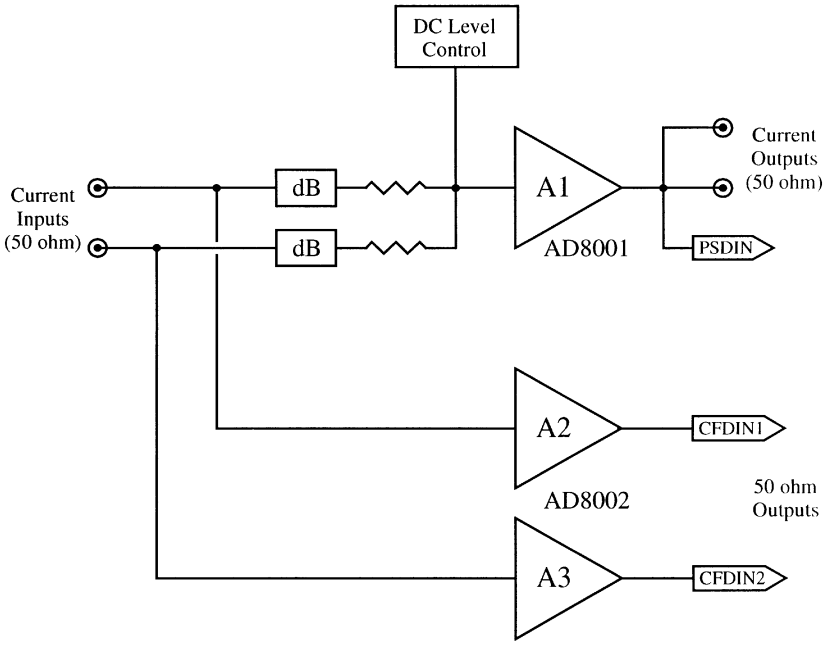

Fig. 3. Block diagram of the analog front-end.

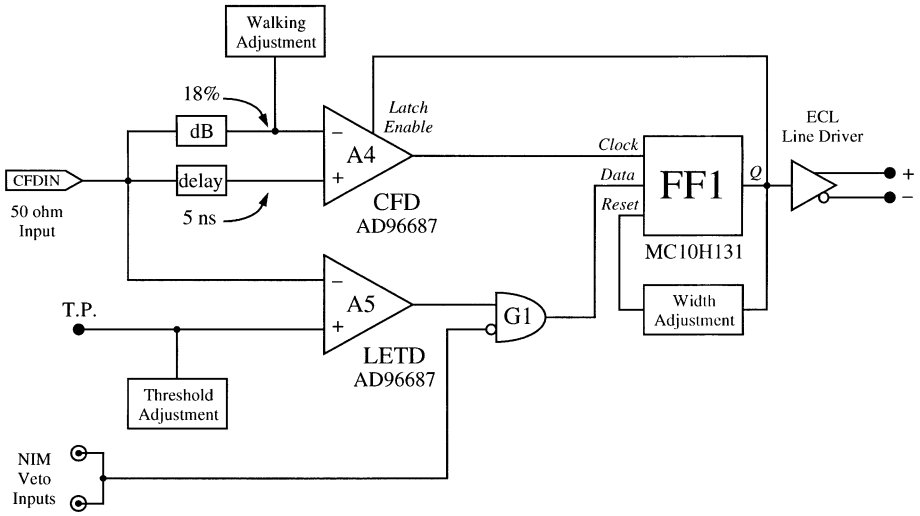

Fig. 4. Block diagram of the constant-fraction discriminator circuit.

amplifier. The PMT signal is first split in two branches, the first going to an attenuator, the second to a removable passive delay line fixed at 5 ns, the PMT pulse rise time. The two branches are then fed directly to the amplifier noninverting and inverting inputs. The circuit works at a constant fraction of the pulse height $f = 18\%$. An adjustable DC level is added to the input to set the minimum time walk (≤ 250 ps) and jitter (≤ 100 ps) of the circuit.

The CFD output signal is fed to the *Clock* input of the D-type flip-flop MC10H131 (FF1), used as pulse former circuit, the output logic level of which is set within an adjustable time window only when a LEDT pulse is present at the input Data. The pulse shaping can be internally adjusted in a range from 15 to 135 ns. During this time, a feedback signal at the Latch Enable input of A4 inhibits the CFD, to avoid updating of the output signal or undesired restarts of FF1.

3.3. Pulse-shape discriminator

The PSD circuit (Fig. 5a) is an electronic evolution of Sperr et al. [14] method: the PMT current signal is integrated and differentiated in a pole-zero-compensated preamplifier OPA640 (A6) so that the zero-cross time of the output pulse depends on the fall time of the input signal.

The RC time constants are experimentally adjusted for best particles discrimination and resolution. The RC integration value is around 30 ns and the differentiation one is chosen in order to have approximately a double-pulse resolution equal to 300 ns.

To detect the baseline crossover of the shaped pulse, an ultrafast comparator AD96687 (A7) is used. A logic gate (G2) is used to form the overlap between the crossover logic pulse and an external strobe signal. Suitably setting the width and the

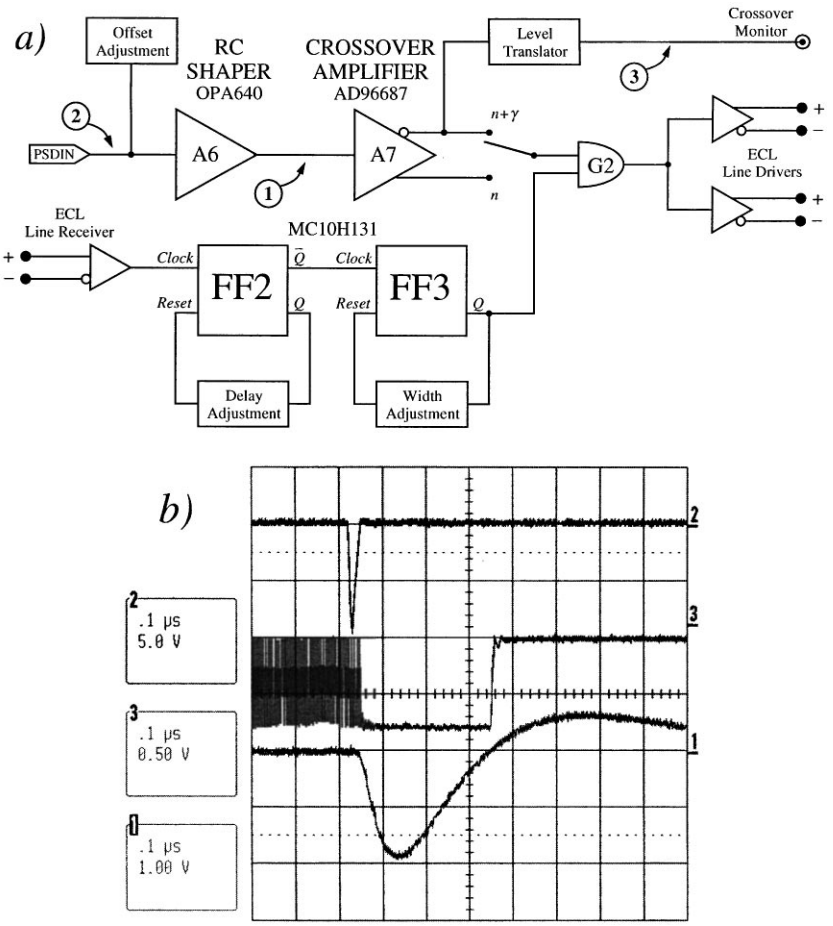

Fig. 5. (a) Block diagram of the pulse-shape discriminator circuit; (b) time relationship between pulses at various points of the circuit.

delay of the strobe signal, a neutron–gamma identification spectrum is generated by G2.

Two D-type flip-flops MC10H131 (FF2, FF3) set the correct strobe parameters. The delay value can be adjusted locally by a front-panel potentiometer in a time ranging from 170 up to 390 ns. The time formation is internally fixed at 100 ns. The time relationship between pulses picked up with a digital graphic oscilloscope at various test points distributed on the PSD circuit can be seen in Fig. 5b. Channels No. 1, 2 and 3 correspond to the shaped pulse, to the input current pulse and to the crossover logic output, respectively. An oscillation of the crossover output, due to the presence of electronic noise, is observed before the arrival of the input signal. This oscillation does not affect the performances of the PSD stage. Anyway, the rejection of this oscillation and the setting of the minimum time jitter (≤ 200 ps) are achieved by an adjustable DC offset ($\pm$ 300 mV) added at the circuit input.

4. Calibration and performances

The calibration of the PSD Unit prototype and the study of the electronics response to fast neutrons and gamma rays were performed using a scintillator counter, 2" diameter, 6" long, manufactured by BICRON, filled with BC501A scintillator, and viewed by two 2" diameter EMI 9964KB03 photomultipliers. The PMT power supplies were set to 1700 V and a 12 dB attenuation of the input anode signals was used. In this condition we were able to record neutron interactions up to 20 MeV energy, which represents the neutron energy upper limit to be studied in Gran Sasso laboratory [2].

The measurements described here were performed in the Pavia laboratory with a 30 mCi Am–Be source. Preliminary results obtained in the Gran Sasso Hall C are also presented. The adopted electronics set-up is shown in Fig. 6. The two PMTs were directly connected to the inputs of the PSD Unit. A coincidence signal was derived from

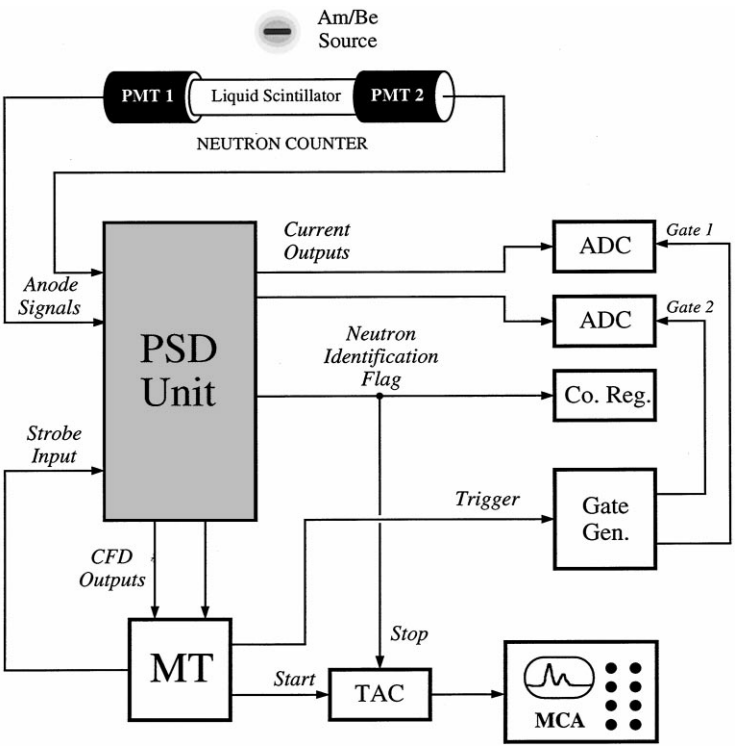

Fig. 6. Electronics set-up used to test the PSD Unit prototype.

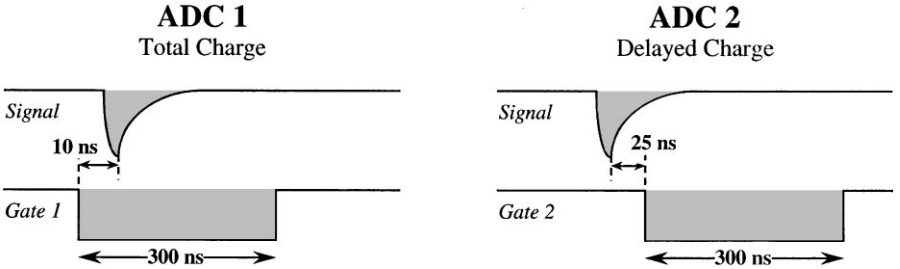

Fig. 7. Timing of the two ADC units used for total and delayed charge measurements.

the two CFD outputs by a meantimer module (MT) [15], the output of which was used to trigger the strobe of the PSD circuit and to trigger the data acquisition system. Two different gates were generated using a PHILLIPS 794 unit (Gate Gen.) and fed in two integrating analog-to-digital converters (ADC) LeCroy 4300B FERA, the inputs of which were connected to the current outputs of the PSD Unit. In Fig. 7 the adopted timing for both total and delayed charge measurements is shown. Since every interacting particle induced a trigger to the data acquisition system, the status of the PSD output was detected and stored using a coincidence register (Co.Reg.) LeCroy 4532 MALU. A Time-to-Amplitude Converter (TAC) ORTEC 566 and a Multi-Channel Analyser (MCA) ORTEC TRUMP were used to measure the PSD response for neutrons and gamma rays, i.e. the time distribution of the delay between the prompt signal issued by the meantimer module and the neutron identification flag.

Two discrimination spectra measured with threshold set at 100 keV recoil electron energy are shown in Fig. 8. The distribution Fig. 8a, acquired with the electronic set-up described here, is compared to the distribution Fig. 8b, where a standard single PMT PSD (CANBERRA 2160A) was used. The advantage of two PMTs light readout for PSD is clear: the corresponding neutron and gamma distributions are less broadened and show a lower asymmetry. This is better characterised by the increase of the peak-to-valley (P/V) ratio, defined as the average of the gamma and neutron peak heights divided by the height of the minimum between them. The main improvement is associated with a better uniformity of the collected light pulse

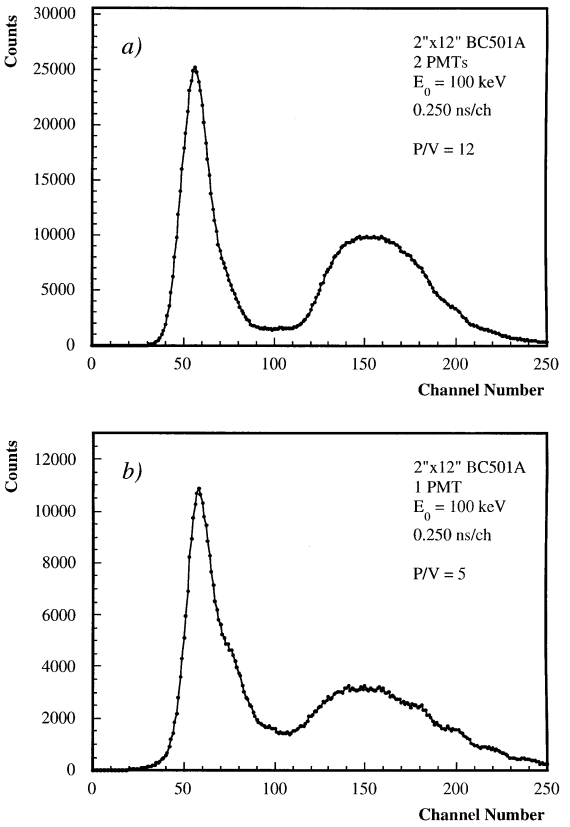

Fig. 8. Neutron–gamma timing distribution spectra with threshold $E_0 = 100$ keV recoil electron energy using two different acquisition systems: (a) two PMTs + meantimer; (b) single PMT + standard electronics.

height spectrum as a function of the interaction point along the cell axis, as shown in Fig. 9. However, the PSD response is also affected by the time resolution optimisation due to the use of the

meantimer unit. Further measurements carried out without compensation of the two PMTs time response, show variations up to 1 ns in the peak widths.

Fig. 10 shows a comparison of PSD spectra at various recoil electron energy thresholds. The best discrimination point, fixed 14 ns far from the gamma peak position, is almost independent of the energy threshold down to 100 keV recoil electron energy. The P/V factor shows a stronger threshold dependence, due to the broadening of the peaks at low-energy deposition [16,17].

To better understand the effectiveness of our system in rejecting the natural gamma ray field, a preliminary neutron measurement was performed in the Gran Sasso Hall C [18]. The plot of the light pulse delayed charge versus the total one, shown in Fig. 11a, is characterised by the presence of two well-separated branches for gamma ray and heavy ionising particle (α, n, p) interactions. The 10 Hz events rate was reduced to 10^{-2} Hz while taking the data rejecting most of the gamma events

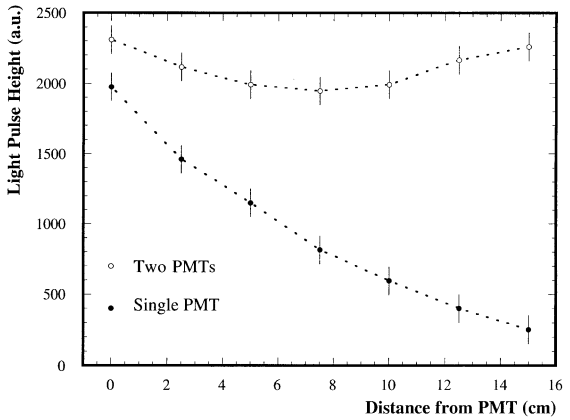

Fig. 9. Light pulse height variation along the 6″ cell axis measured with a collimated ^{137}Cs gamma source. Single PMT and two PMTs (Fan-in/Fan-out output) data are compared.

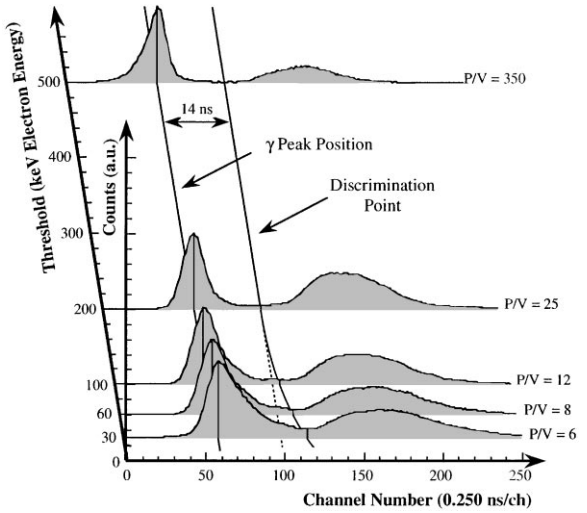

Fig. 10. PSD discrimination spectra measured at various thresholds between 30 and 500 keV recoil electron energy.

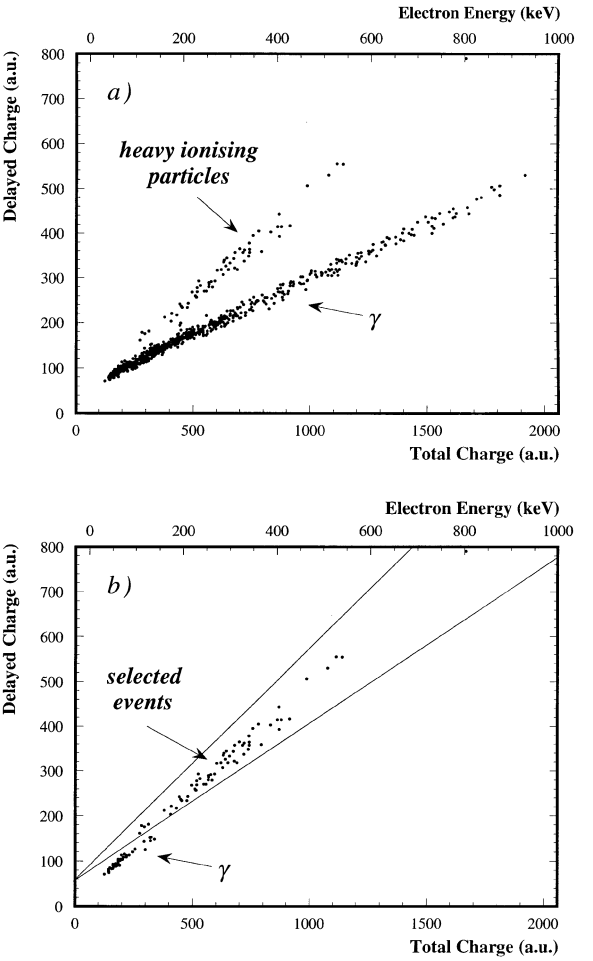

Fig. 11. Two-dimensional spectra of the delayed charge versus the total one measured with the 6″ cell in the Gran Sasso Hall C: (a) total events; (b) PSD selected events.

according to the PSD response. The residual gamma-ray contamination is mainly grouped at energies lower than 100 keV, as shown in Fig. 11b. Processing these events on the basis of the DCC response, as shown in the figure, we got a gamma rejection ratio of $1:10^4$. The precise analysis about the nature of the surviving signals, based on additional constraints in the particle selection [18], has pointed out the presence of very few residual gamma ray events, leaving a final total gamma rejection ratio of $1:10^5$.

5. Conclusions

The results presented here demonstrate the possibility to perform a compact low-cost, high-efficiency neutron–gamma discrimination system. The necessary electronic circuitry, assembled in low-cost NIM modules, owing to their very specific neutron signature, has been proven to accomplish a high rejection of gamma-ray-induced events. Since we have noticed no time or temperature dependence of the threshold position or significant variation of the delay distribution during a one month data taking period, we think this electronic module is very promising for the realisation of big multidetector arrays able to measure low fluxes of fast neutron even in the presence of a significant gamma ray background.

References

[1] ICARUS Collaboration: P. Cennini, S. Cittolin, G. Maurin, A. Placci, J.P. Revol, C. Rubbia, W.H. Tian, J.M. Ma, L.K. Ding, Y. Li, F. Lu, J.F. Qiu, H.Y. Sheng, K.L. Tung, J.Y.Zeng, B. Zhang, F. Casagrande, D. Dzialo Giudice, X. Li, G. Mannocchi, S. Motto, P. Picchi, P. Boccaccio, F. Cavanna, E. Olejarczyk, G. Piano Mortari, M. Verdecchia, D. Cline, W. Hong, G. Muratori, S. Otwinowski, J. Park, H.G. Wang, M. Zhou, A. Bettini, S. Centro, C. De Vecchi, A. Pepato, F. Pietropaolo, S. Ventura, P. Benetti, E. Calligarich, S. Cesana, R. Dolfini, A. Gigli Berzolari, F. Mauri, L. Mazzone, C. Montanari, A. Piazzoli, A. Rappoldi, G.L. Raselli, M. Rossella, D. Scannicchio, M. Terrani, C. Vignoli, F. Sergiampietri, L. Periale, S. Suzuki, E. Fenyves, A first 600 ton ICARUS detector installed at the Gran Sasso Laboratory, addendum, LNGS Report LNGS-95/10 May 1995.

[2] R. Dolfini, M. Maris, C. Montanari, A. Rappoldi, C. Vignoli, A. Borio di Tigliole, A. Cesana, M. Terrani, F. Cavanna, G. Nurzia, F. Pietropaolo, Study of solar neutrino detection in the 600 liquid argon ICARUS time projection chamber, LNGS Report INFN/AE-97/49, 1997.

[3] A. Rindi et al., Nucl. Instr. and Meth. A 272 (1988) 871.

[4] P. Belli et al., Nuovo Cimento A 101 (1989) 959.

[5] R. Aleksan et al., Nucl. Instr. and Meth. A 274 (1989) 203.

[6] S. Affatto, Nuovo Cimento A 104 (1991) 437.

[7] A. Bertin et al., Nucl. Instr. and Meth. A 337 (1994) 445.

[8] D. Wolski et al., Nucl. Instr. and Meth. A 360 (1995) 584.

[9] S. Matsuyama et al., Nucl. Instr. and Meth. A 372 (1996) 246.

[10] BICRON Corporation, USA, BC501A Data Sheet.

[11] F. Arneodo, F. Cavanna, O. Consorte, S. Parlati, G. Piano Mortari, C. Rossi, A. Borio di Tigliole, A. Cesana, M. Terrani, R. Dolfini, R. Nardò, A. Rappoldi, G.L. Raselli, M. Rossella, C. Vignoli, Calibration of BC501A Liquid Scintillator Cells with Monochromatic Neutron Beams, Preprint ICARUS-TM-97/08, 18 july 1997, Nucl. Instr. and Meth., submitted.

[12] P. Netter et al., Nucl. Instr. and Meth. 185 (1981) 165.

[13] R.B. Piercey et al., IEEE Trans. Nucl. Sci, NS-34 (1) (1987) 82.

[14] P. Sperr et al., Nucl. Instr. and Meth. 116 (1974) 55.

[15] A. Cavestro et al., Nucl. Instr. and Meth. A 305 (1991) 488.

[16] M. Moszynski et al., Nucl. Instr. and Meth. A 317 (1992) 262.

[17] M. Moszynski et al., Nucl. Instr. and Meth. A 350 (1994) 226.

[18] F. Arneodo, F. Cavanna, S. Parlati, G. Piano Mortari, C. Rossi, E. Tatananni, M. Verdecchia, A. Borio di Tigliole, A. Cesana, M. Terrani, R. Dolfini, R. Nardò, A. Rappoldi, G.L. Raselli, M. Rossella, C. Vignoli, Underground Neutron Spectrometry with a Liquid Scintillator Detector, LNGS Report INFN/AE-97/52, 1997.